Comparing Remnant Properties from Horizon Data and Asymptotic Data in Numerical Relativity

Dante A. B. Iozzo [ID],[1, *] Neev Khera [ID],[2] Leo C. Stein [ID],[3, †] Keefe Mitman [ID],[4] Michael Boyle [ID],[1] Nils Deppe [ID],[4] François Hébert [ID],[4] Lawrence E. Kidder [ID],[1] Jordan Moxon [ID],[4] Harald P. Pfeiffer [ID],[5] Mark A. Scheel [ID],[4] Saul A. Teukolsky [ID],[4, 1] and William Throwe [ID][1]

[1] *Cornell Center for Astrophysics and Planetary Science, Cornell University, Ithaca, New York 14853, USA*
[2] *Institute for Gravitation and the Cosmos & Physics Department, Penn State, University Park, Pennsylvania 16802, USA*
[3] *Department of Physics and Astronomy, University of Mississippi, University, Mississippi 38677, USA*
[4] *Theoretical Astrophysics 350-17, California Institute of Technology, Pasadena, California 91125, USA*
[5] *Max Planck Institute for Gravitational Physics (Albert Einstein Institute), Am Mühlenberg 1, Potsdam 14476, Germany*
(Dated: June 16, 2021)

We present a new study of remnant black hole properties from 13 binary black hole systems, numerically evolved using the Spectral Einstein Code. The mass, spin, and recoil velocity of each remnant were determined quasi-locally from apparent horizon data and asymptotically from Bondi data $(h, \psi_4, \psi_3, \psi_2, \psi_1)$ computed at future null infinity using SpECTRE's Cauchy characteristic evolution. We compare these independent measurements of the remnant properties in the bulk and on the boundary of the spacetime, giving insight into how well asymptotic data are able to reproduce local properties of the remnant black hole in numerical relativity. We also discuss the theoretical framework for connecting horizon quantities to asymptotic quantities and how it relates to our results. This study recommends a simple improvement to the recoil velocities reported in the Simulating eXtreme Spacetimes waveform catalog, provides an improvement to future surrogate remnant models, and offers new analysis techniques for evaluating the physical accuracy of numerical simulations.

I. INTRODUCTION

One particularly important object of study for gravitational-wave astronomy is the remnant black hole that results from a compact binary coalescence. We are now regularly observing gravitational-wave events, with 50 detections on record so far [1–4]. Identifying the properties of the remnants from observational data can have important astrophysical implications [5–11], and remnant properties have already been used in tests of general relativity (GR) [12–18]. It is therefore critical for numerical simulations to compute these properties with sufficient accuracy. The increased sensitivity of third-generation gravitational-wave detectors will require more accurate waveforms from numerical relativity (NR) [19]. This motivates analyses that not only test numerical convergence but also provide an estimate of the error that corresponds to the underlying physics.

The most common approach for providing remnant properties in NR waveform catalogs uses only local measurements on the remnant apparent horizon [20–23]. The issue with this approach is that the apparent horizon is inherently gauge dependent, and the mass and spin are properly defined only for a Kerr spacetime [24]. It has been shown that numerical simulations do approach a Kerr spacetime during ringdown [25–27], which has allowed for computation of a reliable quasi-local mass and spin in NR [24, 28–34]. An accurate and robust computation of the recoil velocity is more complicated [33, 35],

since a horizon-based definition is entirely dependent on simulation coordinates.

An alternative approach to quasi-local horizon-based definitions is to use conservation laws at future null infinity $\mathscr{I}^+$ to compute the remnant properties asymptotically. The high degree of symmetry in an asymptotically flat region allows for a greater understanding of the gauge freedoms and their effects on the remnant properties [36, 37]. This would provide a more reliable measure of the recoil velocity and provide an independent test of the horizon-based mass and spin measures. While some work has been done to compute the recoil velocity using only the strain waveform of a numerically evolved spacetime [29, 38–42], the lack of curvature information from the Weyl scalars at the asymptotic boundary has prevented a more complete and robust analysis. Most recently, computing the recoil velocity from an asymptotic strain waveform has been applied in the construction of surrogate remnant models [38, 39, 43].

Recent developments have established reliable procedures for computing the gravitational-wave strain h and the Weyl scalars $(\psi_4, \psi_3, \psi_2, \psi_1, \psi_0)$ at $\mathscr{I}^+$ from an NR simulation [44–46]. These asymptotic quantities, collectively known as Bondi data or asymptotic data, are subject to an infinite-dimensional group of gauge freedoms described by the Bondi-Metzner-Sachs (BMS) group [47, 48], which is an enlargement of the Poincaré group. The elements of the BMS group act by transforming the frame of measurement of the asymptotic data, i.e. the Bondi frame. By a careful selection of the Poincaré freedom of the Bondi frame, we can use the BMS charges to determine the remnant properties asymptotically [49–52].

We present the first asymptotic measurements of the

arXiv:2104.07052v2 [gr-qc] 15 Jun 2021

mass, spin, and recoil velocity of remnant black holes in NR using the full set of asymptotic data. We are able to determine the mass and recoil velocity of the remnant from the Bondi energy-momentum vector. The total angular momentum charge contains a spin contribution and an orbital angular momentum contribution. By isolating the spin contribution we can compute the spin vector of the remnant. These asymptotic remnant properties are compared to the horizon-based remnant properties. For this study, we use the same procedure for computing the horizon-based remnant properties as is used for the Simulating eXtreme Spacetimes (SXS) waveform catalog [22, 30, 53].

Comparing the remnant properties measured in the bulk of the spacetime from the remnant apparent horizon and on the boundary of the spacetime provides a test of how well the asymptotic data are able to reproduce local properties of the remnant black hole. We perform this comparison on a set of 13 binary black hole (BBH) systems numerically evolved using the Spectral Einstein Code (SpEC) [54]. The initial parameters of these systems have been selected to cover a range of mass ratios and initial spin configurations. The asymptotic data are computed using SpECTRE's [44] next-generation Cauchy characteristic extraction (CCE) code [45, 55–57].

We find that the measurement of the recoil velocity and the spin from the asymptotic data demonstrates a nontrivial sensitivity to Poincaré transformations. This sensitivity becomes problematic because of the drift of the center of mass (CoM) during the numerical evolution [22, 58–61], which results in the horizon-based recoil velocity, the asymptotic recoil velocity, and the asymptotic spin being measured in an undesirable Poincaré frame. We demonstrate the effectiveness of an established procedure to correct for the CoM drift [58].

Further, through this study we show a good agreement between the horizon-based and asymptotic measurements, especially for the mass and spin. We argue that our asymptotic recoil velocity provides a much more reliable measurement than both the horizon-based one and the one computed for surrogate remnant models [39]. Unfortunately, the SXS simulation catalog [53] does not yet contain the full set of asymptotic data that is necessary to properly compute the asymptotic recoil velocity. Until the full set of asymptotic data is available, we suggest a simple and temporary improvement to the horizon-based recoil velocity currently being reported in the catalog.

In this paper, we identify a four-vector with lowercase Latin indices Y^a, a three-vector with an arrow $\vec{Y}$, and a unit three-vector with a circumflex $\hat{Y}$. The Euclidean norm of a previously identified three-vector $\vec{Y}$ will be written as Y.

II. COMPARISON OF REMNANT PROPERTIES

The three remnant black hole properties of interest for this study are the mass, the recoil velocity, and the dimensionless spin. These three properties are currently computed by SpEC from the apparent horizon data and made available[1] as part of the SXS catalog of NR simulations [22, 53]. Although the mass and spin provided in the catalog are expected to be accurate, the recoil velocity is subject to a far greater host of issues since it is computed from a linear fit to the coordinate trajectory of the horizon.

An independent measurement of the remnant properties cannot be determined from the asymptotic gravitational wave strain h alone. Rather, the asymptotic Weyl scalars $(\psi_4, \psi_3, \psi_2, \psi_1)$ are required for computing appropriate BMS charges and for transforming the asymptotic data into a suitable Poincaré frame. The asymptotic Weyl scalar ψ_0 is not required because ψ_1 is the lowest index Weyl scalar used to compute the BMS charges [49–52]. Although ψ_4 and ψ_3 are not used directly to define the remnant properties, a BMS transformation of a Weyl scalar requires all higher index Weyl scalars [49, 62, 63]. We apply a boost and translation to correct for the CoM drift of the numerical BBH evolution, as discussed in Sec. III.

The asymptotic data $(h, \psi_4, \psi_3, \psi_2, \psi_1)$ on $\mathscr{I}^+$ are determined from SpEC NR simulations by computing the metric and its derivatives on a worldtube of finite radius, and then using the SpECTRE CCE code [44, 45] to solve the full Einstein equations in the region between that worldtube and $\mathscr{I}^+$. Consequently, as shown below, we are now able to determine the remnant properties from the asymptotic data itself, independent from any horizon-based measurements.

A. Local Remnant Properties

The values for the dimensionless remnant spin $\vec{\chi}_\mathcal{H}$ and remnant mass $M_\mathcal{H}$ in the SXS catalog are currently computed from the properties of the remnant apparent horizon $\mathscr{H}$. Before proceeding to identify the properties of the remnant black hole, we first define the properties computed from an apparent horizon in general.

The black hole during ringdown is highly dynamical and not axially symmetric. Late into ringdown it settles down sufficiently to allow meaningful horizon-based quantities to be defined [25–27]. However, during the ringdown we can still find the three approximate rotational Killing vector fields (KVFs), tangent to $\mathscr{H}$, that are closest to satisfying the Killing equation [22, 64, 65]. We then compute the three components of the spin angular momentum,

---

[1] These remnant properties are available in the `metadata.txt` and `metadata.json` files for each simulation.

$(S_{(1)}, S_{(2)}, S_{(3)})$, generated by the three approximate rotational KVFs. With this, the spin magnitude S of the apparent horizon is defined by

$$S \equiv \sqrt{S_{(1)}^2 + S_{(2)}^2 + S_{(3)}^2}. \tag{1}$$

Unlike the spin magnitude, the spin axis cannot be defined unambiguously because of the coordinate freedom of GR [30]. The measure of the spin axis in SpEC is

$$\hat{\chi}_{\mathcal{K}} = \frac{1}{N} \int_{\mathscr{H}} \vec{r} \, \mathrm{Im}(\mathcal{K}) \, dA, \tag{2}$$

where $\vec{r}$ is the Euclidean position vector in simulation coordinates, N is a normalization factor, and $\mathcal{K}$ is the Penrose-Rindler complex curvature of $\mathscr{H}$ [30, 66]. Together, S and $\hat{\chi}_{\mathcal{K}}$ can be used to define the dimensionless spin once a mass quantity has been defined.

We may then define the Christodoulou mass, which is derived from the apparent horizon area [67]. The Christodoulou mass is only properly defined for stationary spacetimes, but the Christodoulou-Ruffini equation is used here to define at least a quasi-local measure of the horizon mass,

$$M_{\mathrm{Ch}}^2 \equiv M_{\mathrm{irr}}^2 + \frac{S^2}{4M_{\mathrm{irr}}^2}, \tag{3}$$

where the irreducible mass M_{irr} is computed by an area integral over the horizon,

$$M_{\mathrm{irr}}^2 \equiv \frac{1}{16\pi} \int_{\mathscr{H}} dA. \tag{4}$$

The Christodoulou mass is also used for defining the mass of the BBH system M, which is the sum of M_{Ch} for each black hole as measured at the earliest time in the simulation after the junk radiation passes the outer boundary of the domain.[2]

To identify the values of spin and mass of the remnant black hole, we compute a time-average of the values late into the ringdown when the black hole is approximately Kerr. At such a late time in the ringdown, the values of mass and spin are approximately constant in time to a fraction of a percent, so time-averaging is not strictly necessary; nevertheless, we use the time-average procedure to remove the need to choose a particular time and to average over any remaining numerical noise. The ringdown phase of the simulation starts when the earliest common apparent horizon is detected (at simulation time $t = t_{\mathrm{RD}}$) and ends when most of the radiation leaves the domain. In practice, the final time of the simulation is

$$t_f = t_{\mathrm{RD}} + r_{\mathrm{max}} + 100\,M, \tag{5}$$

where r_{max} is the radius of the outer boundary of the computational domain. The values of S, $\hat{\chi}_{\mathcal{K}}$, and M_{Ch} are computed on a densely sampled set of times in the last third of the ringdown phase. The dimensionless remnant spin $\vec{\chi}_{\mathcal{H}}$ and remnant mass $M_{\mathcal{H}}$ are defined to be the time-averaged values on this dense set of times,

$$M_{\mathcal{H}} = \frac{1}{t_f - t_0} \int_{t_0}^{t_{\mathrm{f}}} M_{\mathrm{Ch}}(t) \, dt, \tag{6a}$$

$$\vec{\chi}_{\mathcal{H}} = \frac{1}{t_f - t_0} \int_{t_0}^{t_{\mathrm{f}}} \frac{S(t)}{M_{\mathrm{Ch}}(t)^2} \hat{\chi}_{\mathcal{K}}(t) \, dt, \tag{6b}$$

where t_0 is the start of the last third of the ringdown phase.

The velocity of the apparent horizon is defined by the coordinate trajectory of the horizon center. It is therefore more susceptible to gauge effects than the mass and spin. The apparent horizon coordinate center $\vec{x}(t)$ is defined to be the surface-area weighted average of the location of the spatial cross-section of the horizon $\mathscr{H}_t$,

$$\vec{x}(t) = \frac{1}{A} \int_{\mathscr{H}_t} \vec{r} \, dA, \tag{7}$$

where A is the surface area of $\mathscr{H}_t$. Over the last third of the ringdown phase, we model $\vec{x}(t)$ with a least-squares fit to a linear function of time. The time derivative of this fit is the coordinate recoil velocity

$$\vec{V}_{\mathcal{H}} = \partial_t \langle \vec{x} \rangle(t), \tag{8}$$

where $\langle \vec{x} \rangle(t)$ is the linear least-squares fit of $\vec{x}(t)$.

B. Asymptotic Remnant Properties

In contrast to the quasi-local definitions of the horizon properties, we can compute the properties of the remnant black hole using information stored in the asymptotic data on $\mathscr{I}^+$ [49]. The asymptotic remnant mass M_∞ and recoil velocity $\vec{V}_\infty$ can be identified from the Bondi energy-momentum vector P_{B}^a, which is computed from ψ_2 and the asymptotic Newman-Penrose shear σ. The asymptotic remnant spin $\vec{\chi}_\infty$ can be identified from the Bondi angular momentum vector $\vec{J}_{\mathrm{B}}$, computed from ψ_1 and σ. Using our conventions,[3] we can identify the asymptotic gravitational-wave strain with the complex conjugate of the Newman-Penrose shear: $h = \bar{\sigma}$.

Consider a foliation of $\mathscr{I}^+$ parametrized by a Bondi time coordinate u such that each slice is an S^2 surface of constant $u \equiv t - r$. This foliation is not unique; other foliations on constant $\tilde{u} = u + \alpha(\theta, \phi)$ for any smooth function $\alpha(\theta, \phi)$ are also possible. The transformations

---

[2] This time is known as the *reference time* in the SXS catalog metadata [22].

[3] This relation is only valid asymptotically. Yet even then it is not valid in every convention. See Appendix C of [46] for details.

that take the constant u foliation into the constant $\tilde{u}$ foliation are called supertranslations and form an important subgroup of the BMS group.[4] On each of the S^2 slices, we can define the Bondi mass aspect

$$m = -\mathrm{Re}\left(\psi_2 + \sigma\dot{\bar{\sigma}}\right), \qquad (9)$$

where the overdot signifies a derivative with respect to u. By projecting m along the different components of the outgoing null tetrad vector $l^a = (1, \sin\theta\cos\phi, \sin\theta\sin\phi, \cos\theta)$, we can compute the Bondi energy-momentum vector

$$P_{\mathrm{B}}^a = \frac{1}{4\pi}\int l^a m \, d\Omega. \qquad (10)$$

From here, it is straightforward to compute the Bondi rest mass

$$M_{\mathrm{B}} = \sqrt{-P_{\mathrm{B}}^a P_{\mathrm{B}}^b \eta_{ab}}, \qquad (11)$$

where η_{ab} is the $(-,+,+,+)$ Minkowski metric. Analogous to the energy-momentum vector in special relativity, a Bondi velocity $\vec{V}_{\mathrm{B}}$ can be defined by

$$\vec{V}_{\mathrm{B}} = \frac{\vec{P}_{\mathrm{B}}}{P_{\mathrm{B}}^0}. \qquad (12)$$

The calculation of the asymptotic spin vector is more involved. The total angular momentum charge $\vec{J}_{\mathrm{B}}$ contains a contribution from both the orbital and spin angular momenta. The orbital contribution arises when the remnant is boosted and translated with respect to the origin. Additionally, if the recoil velocity is not aligned with the spin axis then the components of the spin orthogonal to the velocity will be Lorentz transformed. In a center-of-momentum (CoMom) frame, however, the orbital contribution will vanish and the total angular momentum vector can be identified as the spin vector determined in the expected frame.

We can use the transformation of angular momentum under a boost to compute the angular momentum vector in a CoMom frame. Along with $\vec{V}_{\mathrm{B}}$, this procedure requires the total angular momentum charge $\vec{J}_{\mathrm{B}}$ and the boost charge $\vec{K}_{\mathrm{B}}$,

$$\vec{J}_{\mathrm{B}} = \frac{1}{4\pi}\int \mathrm{Im}\left(\bar{\eth}\hat{r}N\right)\, d\Omega, \qquad (13\mathrm{a})$$

$$\vec{K}_{\mathrm{B}} = \frac{1}{4\pi}\int \mathrm{Re}\left(\bar{\eth}\hat{r}N\right)\, d\Omega, \qquad (13\mathrm{b})$$

where $\hat{r} = (\sin\theta\cos\phi, \sin\theta\sin\phi, \cos\theta)$, $\eth$ is the Geroch-Held-Penrose spin-weight raising operator [68], and N is the "Lorentz aspect",

$$N = -\left(\psi_1 + \sigma\eth\bar{\sigma} + \frac{1}{2}\eth\left(\sigma\bar{\sigma}\right) + u\eth m\right). \qquad (14)$$

With these charge vectors in hand, we can now compute the asymptotic dimensionless spin vector

$$\vec{\chi}_{\mathrm{B}} = \frac{\gamma}{M_{\mathrm{B}}^2}\left(\vec{J}_{\mathrm{B}} + \vec{V}_B \times \vec{K}_{\mathrm{B}}\right) - \frac{\gamma - 1}{M_{\mathrm{B}}^2}\left(\hat{V}_B \cdot \vec{J}_{\mathrm{B}}\right)\hat{V}_B, \qquad (15)$$

where γ is the Lorentz factor [69]. In general, Eqs. (13) and (15) depend on the Bondi frame, but as the asymptotic data approaches stationarity at late times, Eq. (15) stops depending on the frame and becomes unambiguous. See the Appendix for details.

It turns out that the values of M_{B}, $\vec{V}_{\mathrm{B}}$, and $\vec{\chi}_{\mathrm{B}}$ computed from CCE waveforms are relatively constant over the last half of the ringdown phase in the simulation. The deviation is almost two orders of magnitude smaller than the differences between the asymptotic and horizon quantities we are interested in comparing. Therefore, we take the values of M_B, $\vec{V}_{\mathrm{B}}$, and $\vec{\chi}_{\mathrm{B}}$ on the last available time in the data, u_f, to be the remnant properties,

$$M_\infty = M_{\mathrm{B}}(u_f), \qquad (16\mathrm{a})$$

$$\vec{V}_\infty = \vec{V}_{\mathrm{B}}(u_f), \qquad (16\mathrm{b})$$

$$\vec{\chi}_\infty = \vec{\chi}_{\mathrm{B}}(u_f). \qquad (16\mathrm{c})$$

An alternative approach is used to compute the asymptotic recoil velocity for surrogate remnant models. These models only had access to the asymptotic strain,[5] which can be used to compute the momentum flux [38, 39, 43, 74],

$$\dot{\vec{P}}_{\mathcal{F}}(u) = \frac{1}{16\pi}\int \vec{l}\,|\dot{\sigma}(u)|^2 d\Omega. \qquad (17)$$

While it is straightforward to numerically integrate the momentum flux, a constant of integration must be chosen. For the surrogates, the antiderivative of the momentum flux $\vec{\mathcal{P}}_{\mathcal{F}}(u)$ is computed using fifth order splines. The integration constant is taken to be the mean value of $\vec{\mathcal{P}}_{\mathcal{F}}(u)$ over the interval $[u_0, u_1]$, chosen to be the first $1000\,M$ of time after the junk radiation has passed. This amounts to a frame choice in which the average value of the momentum is zero for the early part of the waveform. The remnant velocity is then defined to be

$$\vec{V}_{\mathcal{F}} = \frac{1}{M_{\mathcal{H}}}\left(\vec{\mathcal{P}}_{\mathcal{F}}(u_f) - \frac{1}{u_1 - u_0}\int_{u_0}^{u_1}\vec{\mathcal{P}}_{\mathcal{F}}(u')du'\right). \qquad (18)$$

The issue here is that $\vec{\mathcal{P}}_{\mathcal{F}}(u)$ can be significantly oscillatory in the interval $[u_0, u_1]$. The mean value, and hence the value of $\vec{V}_{\mathcal{F}}$, is therefore undesirably sensitive

---

[4] The spacetime translations are the supertranslations for which $\alpha(\theta, \phi)$ is a linear combination of the $\ell \leq 1$ spherical harmonics.

[5] The asymptotic strain used by these models was extracted directly from NR simulations using Regge-Wheeler-Zerilli extraction [70–73]. If one is instead computing the strain from ψ_4, then it would be more straightforward to use Eq. (17) with a time-integral of ψ_4 instead of $\dot{\sigma}$.

to the length of the interval. The sensitivity of $\vec{V}_{\mathcal{F}}$ on the interval length is dependent on how oscillatory $\vec{\mathcal{P}}_{\mathcal{F}}(u)$ is. Conversely, the frame of $\vec{V}_{\infty}$ is chosen so that the initial BBH CoM is at rest. As discussed in Sec. III, the CoM drift in the simulation is corrected by transforming $\vec{V}_{\infty}$ to a frame in which CoM drift averaged over 90% of the inspiral is set to zero [58]. The CoM drift is far less oscillatory and is averaged over a longer interval than $\vec{\mathcal{P}}_{\mathcal{F}}(u)$. We therefore expect that $\vec{V}_{\mathcal{F}}$ will not be as robust as $\vec{V}_{\infty}$, but still more accurate than $\vec{V}_{\mathcal{H}}$.

C. Connecting the horizon to infinity

It is not immediately obvious why the horizon-based quantities $(M_{\mathcal{H}}, \vec{V}_{\mathcal{H}}, \vec{\chi}_{\mathcal{H}})$ defined on $\mathscr{H}$ should agree with the asymptotic quantities $(M_{\infty}, \vec{V}_{\infty}, \vec{\chi}_{\infty})$ defined on $\mathscr{I}^+$. However, since the spacetime asymptotes to Kerr at late times,[6] we can use Killing symmetries to show why the two definitions of mass and total spin angular momentum agree. The argument for the agreement between the two definitions of remnant velocity and spin direction is less rigorous but still provides a plausible explanation that lends a deeper insight into the simulation coordinates.

For the two Killing symmetries of Kerr (time translation and axisymmetry), we can use the Noether charge construction, following [77–80]. This construction starts from a variation of the Lagrangian 4-form $\boldsymbol{L}$ for GR (boldface will denote differential forms). This first order variation is of the form $\delta \boldsymbol{L} = \boldsymbol{E} \delta \phi + d\boldsymbol{\Theta}$, where ϕ denotes all field variables, $\boldsymbol{E} = 0$ are the equations of motion as a 4-form, and the (pre)symplectic potential 3-form $\boldsymbol{\Theta}$, which is built from ϕ and $\delta\phi$, is the "boundary term" that arises from integrating by parts.

Every diffeomorphism, with generator ξ^a, has an associated Noether current 3-form

$$\boldsymbol{j}_{\xi} = \boldsymbol{\Theta}(\phi, \mathcal{L}_{\xi}\phi) - \xi \cdot \boldsymbol{L}. \tag{19}$$

Here $\mathcal{L}_{\xi}$ is the Lie derivative along ξ^a, and $\xi \cdot \boldsymbol{L}$ denotes contracting ξ into the first slot of $\boldsymbol{L}$. The conservation law for this current is

$$d\boldsymbol{j}_{\xi} = -\boldsymbol{E}\,\mathcal{L}_{\xi}\phi, \tag{20}$$

which vanishes when the equations of motion are satisfied, $\boldsymbol{E} = 0$. There is therefore a charge 2-form $\boldsymbol{Q}_{\xi}$ satisfying

$$\boldsymbol{j}_{\xi} = d\boldsymbol{Q}_{\xi} + \xi^a \boldsymbol{C}_a, \tag{21}$$

where $\boldsymbol{C}_a$ are constraints that vanish on shell, i.e. when the equations of motion are satisfied. Then from the generalized Stokes theorem, if Σ is a 3-surface with boundary

---

[6] Beyond the case of quasi-stationary spacetimes discussed here, connecting a dynamical horizon to $\mathscr{I}^+$ is discussed in [75, 76].
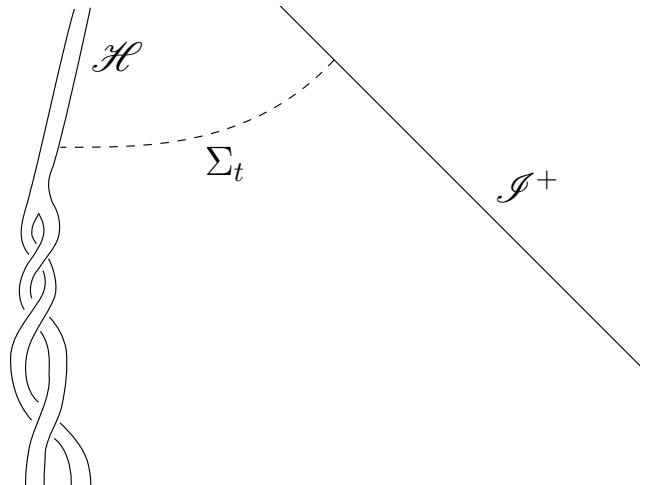

FIG. 1. A diagram of a BBH spacetime, showing the inner boundary formed by the horizon $\mathscr{H}$ and the outer boundary formed by future null infinity $\mathscr{I}^+$. Integrating Eq. (22) over the spacelike hypersurface Σ_t justifies the equality of the horizon quantities and asymptotic quantities.

$\partial\Sigma$, we have the equality

$$\int_{\Sigma} \boldsymbol{j}_{\xi} = \int_{\partial\Sigma} \boldsymbol{Q}_{\xi}, \tag{22}$$

when evaluated on shell.

Note that while $\boldsymbol{Q}_{\xi}$ is ambiguously defined, we make the choice to define it as in [81] with

$$\boldsymbol{Q}_{\xi} = -\frac{1}{8\pi} \star d\boldsymbol{\xi}, \tag{23}$$

where $\star$ is the Hodge star operator.

So far this formalism applies to any diffeomorphism, but something special happens for isometries in vacuum GR. When ξ is a KVF, $\mathcal{L}_{\xi}\phi = 0$ for all fields. This makes the first term in Eq. (19) vanish. Also, the Lagrangian is proportional to the Ricci scalar, which vanishes in vacuum. This makes the second term in Eq. (19) vanish, so $\boldsymbol{j}_{\xi} = 0$ on shell. Additionally, while Eq. (22) in general depends on the vector field off $\mathscr{I}^+$, or is 'gauge dependent,' this problem does not arise for Killing vectors [82].

Now choose Σ_t to be a spacelike hypersurface as depicted in Fig. 1. The surface Σ_t intersects the horizon $\mathscr{H}$ and asymptotes to null as it approaches $r \to \infty$, so that it intersects $\mathscr{I}^+$. If we now excise the region inside $\mathscr{H}$, the boundary $\partial\Sigma_t$ has two spherical components: $\mathscr{H}_t = \Sigma_t \cap \mathscr{H}$ and $\mathscr{B}_t = \Sigma_t \cap \mathscr{I}^+$. Inserting this into the result from Stokes' theorem in Eq. (22), and using the fact that $\boldsymbol{j}_{\xi}$ vanishes for an isometry, we see that

$$0 = -\int_{\mathscr{H}_t} \boldsymbol{Q}_{\xi} + \int_{\mathscr{B}_t} \boldsymbol{Q}_{\xi}, \tag{24}$$

where the sign flip on the first term is because the sphere $\mathscr{H}_t$ has normal pointing toward increasing r, which is negatively oriented in the sense that it points into Σ_t.

Since Eq. (23) is closed for Killing vectors in vacuum, the integrals are independent of the cross-sections picked for $\mathscr{H}_t$ and $\mathscr{B}_t$.

The question remains as to how these integrals are related to the horizon and BMS charges. While for asymptotic symmetries at $\mathscr{I}^+$ the relation of the integral to the BMS charges is highly nontrivial, for Killing vectors it is straightforward [82], where we get half the Bondi rest mass for time translation and the Bondi angular momentum for the rotations [81]. On the other hand the quasi-local horizon charges are only defined in the presence of the Killing fields inspired by such charge integrals.

From this result, we can show that the horizon and asymptotic definitions of mass and total spin angular momentum should agree. At sufficiently late times, as the spacetime approaches that of a boosted Kerr black hole with a decaying amount of radiation, the spacetime will acquire the symmetries of Kerr, namely time translation and axisymmetry. The appropriately normalized generator ∂_ϕ will give the Euclidean norm of the Bondi angular momentum when $\boldsymbol{Q}_{\partial_\phi}$ is evaluated on $\mathscr{B}_t$, and the magnitude S given in Eq. (1) when evaluated on $\mathscr{H}_t$. Although in practice we may use a different ∂_ϕ to define angular momentum at $\mathscr{B}_t$ in Eq. (13a) (due to the supertranslation freedom), all choices of ∂_ϕ give the same angular momentum, as discussed in the Appendix. Similarly, if we take the ∂_t generator, we will find the equality between the Bondi mass and the Christodoulou mass.

A different argument is necessary to explain the agreement of the remnant velocity and the direction of the spin vector. For example, one could imagine coordinates that have an r-dependent rotation between the horizon and infinity. Apparently, our gauge choice makes the coordinate system sufficiently rigid that there is no such relative rotation to offset the horizon and asymptotic spin vectors. We can speculate that this is due to two properties of damped harmonic (DH) gauge [84–86]. First, in a stationary region of $\mathscr{I}^+$, like at late times, there is a canonical Poincaré subgroup of the BMS group. As we approach $r \to \infty$, the DH coordinates approach harmonic Cartesian coordinates, which are compatible with the preferred Poincaré subgroup. Second, in the strong-field, the DH gauge source functions are dominated by their dependence on metric components, rather than explicitly on coordinate functions. This suggests that there are no preferred directions introduced by the DH gauge choice, though it may be affected by physically preferred directions; for example, frame dragging can affect coordinates. Together, these two properties may explain how the DH gauge rigidly connects coordinates in the strong field region to the preferred coordinates of asymptotic infinity, and thus may explain why horizon and asymptotic definitions of spin direction and remnant velocity agree.

III. RESULTS

For this study, 13 binary black hole mergers were numerically evolved using SpEC [54]. The initial parameters of these BBH systems are listed in Table I, and each system was evolved with three different levels of resolution to ensure the convergence of the results. The results presented in this paper are from the highest resolution simulations. For the purpose of estimating the numerical error, we have included comparisons of the highest resolution with the second-highest resolution simulations. The second-highest resolution results will be marked by a superscript "LowRes". To obtain the asymptotic data, the metric and its derivatives were first computed on a worldtube of radius $8.5\lambda_0$, where λ_0 is the initial reduced gravitational wavelength as determined by the orbital frequency of the binary from the initial data. Then Einstein's equations were solved between this worldtube and $\mathscr{I}^+$ using the SpECTRE CCE code [44, 45], and the asymptotic data were computed using the CCE solution at $\mathscr{I}^+$. All calculations involving asymptotic quantities were performed with the scri python module [62, 87–89].

There is a known center-of-mass (CoM) drift during the Cauchy evolution in SpEC [22, 58–61]. This drift results in a boost and a translation of the numerical coordinate system (including coordinates on $\mathscr{I}^+$) relative to the CoM, and this boost and translation will affect the asymptotically-measured remnant spin and recoil velocity (but not the remnant mass, which is defined as the Lorentz-invariant rest mass). To ensure that the remnant spin and recoil velocity are being measured in the CoM frame, the procedure outlined in Ref. [58] has been applied to all the asymptotic data used in this study, before any asymptotic remnant properties are computed. This procedure attempts to transform the asymptotic data to the CoM frame and reduce these gauge effects.

Regarding the apparent horizon properties, even though the CoM drift does not affect $M_\mathcal{H}$ and $\vec{\chi}_\mathcal{H}$, it does have an effect on $\vec{V}_\mathcal{H}$ because $\vec{V}_\mathcal{H}$ is purely coordinate defined. To correct for the effects of CoM drift on $\vec{V}_\mathcal{H}$, we apply the boost used in the CoM correction for the asymptotic data to $\vec{V}_\mathcal{H}$ (see Eq. (25) below). At the time of writing, such a CoM correction has not previously been applied to recoil velocities in the SXS waveform catalog,[7] so the current recoil velocity in the catalog is actually $\vec{V}_{\mathcal{H},\text{raw}}$ (the subscript "raw" will be used to signify recoil velocity measurements without a CoM correction).

In all of the following plots, the ordering of the simulations on the horizontal axis is sorted by the value of V_∞ from smallest to largest.

---

[7] In the SXS waveform catalog's metadata.txt files, the value for the new entry coord-remnant-velocity will be CoM-corrected but the value for raw-coord-remnant-velocity (called remnant-velocity at the time of writing) is not.

Name	q	$\vec{\chi}_A$:	$(\hat{x},$	$\hat{y},$	$\hat{z})$	$\vec{\chi}_B$:	$(\hat{x},$	$\hat{y},$	$\hat{z})$
q1_nospin	1.0		(0,	0,	0)		(0,	0,	0)
q1_aligned_chi0_2	1.0		(0,	0,	0.2)		(0,	0,	0.2)
q1_aligned_chi0_4	1.0		(0,	0,	0.4)		(0,	0,	0.4)
q1_aligned_chi0_6	1.0		(0,	0,	0.6)		(0,	0,	0.6)
q1_antialigned_chi0_2	1.0		(0,	0,	0.2)		(0,	0,	−0.2)
q1_antialigned_chi0_4	1.0		(0,	0,	0.4)		(0,	0,	−0.4)
q1_antialigned_chi0_6	1.0		(0,	0,	0.6)		(0,	0,	−0.6)
q1_precessing	1.0		(0.487,	0.125,	−0.327)		(−0.190,	0.051,	−0.227)
q1_superkick	1.0		(0.6,	0,	0)		(−0.6,	0,	0)
q4_nospin	4.0		(0,	0,	0)		(0,	0,	0)
q4_aligned_chi0_4	4.0		(0,	0,	0.4)		(0,	0,	0.4)
q4_antialigned_chi0_4	4.0		(0,	0,	0.4)		(0,	0,	−0.4)
q4_precessing	4.0		(0.487,	0.125,	−0.327)		(−0.190,	0.051,	−0.227)

TABLE I. Initial parameters of the BBH systems studied in this paper. The mass ratio is $q = M_A/M_B$, and the initial dimensionless spins of the two black holes are $\vec{\chi}_A$ and $\vec{\chi}_B$. These systems all begin orbiting in the x-y plane. For further details, see [83]. The waveforms from these systems are made publicly available at [53].
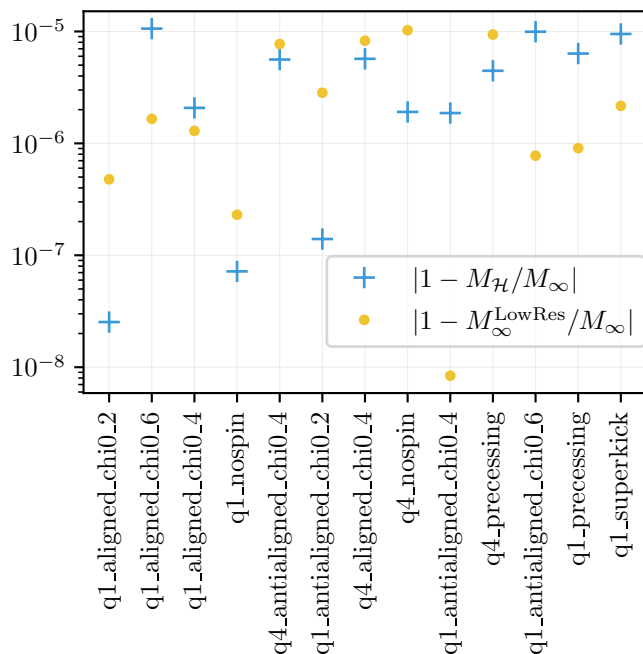

FIG. 2. The relative difference between the remnant mass computed by horizon-based quantities and by asymptotic quantities for several different numerically evolved BBH systems. The data represented by yellow dots provide a measure of the numerical error by comparing the asymptotic remnant mass between resolutions. This plot shows whether the dominant source of error comes from numerical resolution or the methods used to compute the mass. See Table I for the initial parameters of each system.

asymptotic data M_∞ for each of the 13 BBH simulations is plotted in Fig. 2. Overall, we find that there is good agreement on the value of the remnant mass. For nearly equal-mass systems with low spin, we find a relative difference of about $\mathcal{O}(10^{-7})$ between $M_\mathcal{H}$ and M_∞. For more complicated systems, we find the relative difference ranging between $\mathcal{O}(10^{-6})$ and $\mathcal{O}(10^{-5})$. Because the value of the asymptotic remnant mass is defined to be the Bondi rest mass, we can expect this quantity to be invariant to the Poincaré transformation of a CoM correction. That being the case, it makes a negligible difference whether the asymptotic data were CoM-corrected or not.

The numerical error is taken to be the difference of the asymptotic mass between simulations with different numerical resolutions. Because of the rapid convergence of spectral methods, this error measure usually overestimates the actual error in the highest-resolution simulation, but it can nonetheless provide general insight in comparing horizon-based and asymptotic mass with respect to the resolution error. The numerical error in the mass is not consistent across the BBH systems. The difference between horizon-based and asymptotic mass is substantially larger than the resolution error for fewer than half of the systems.

As discussed in Sec. II C, we can expect a good agreement between the horizon-based and asymptotic mass. At the same time, however, there is no clear indication which is the more "physically accurate" value of the mass. Thus, Fig. 2 primarily identifies whether the dominant source of error is from numerical resolution of the simulation or from the computation of the mass itself.

A. Mass Comparison

The relative difference between the remnant black hole mass computed from the horizon data $M_\mathcal{H}$ and from the

B. Recoil Velocity Comparison

The recoil velocity $\vec{V}_\mathcal{H}$ computed from a linear fit of the apparent horizon trajectory is entirely dependent on
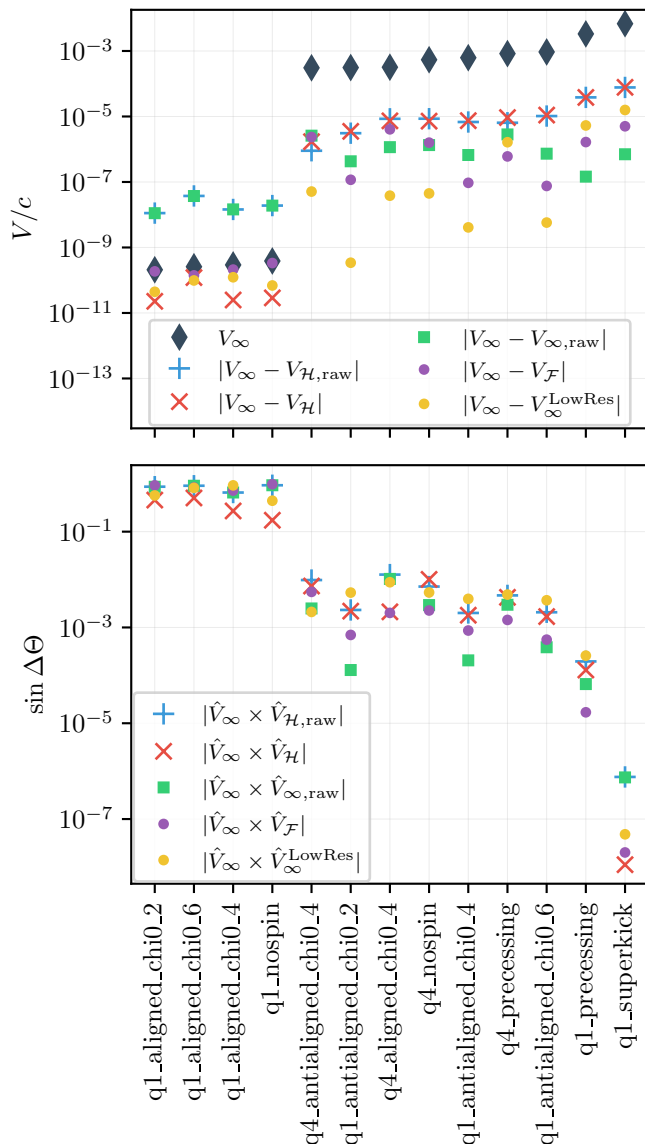
FIG. 3. A comparison of the CoM-corrected asymptotic recoil velocity $\vec{V}_\infty$ with the CoM-corrected apparent horizon recoil velocity $\vec{V}_\mathcal{H}$ and the same recoil velocity measurements without the CoM correction, $\vec{V}_{\infty,\mathrm{raw}}$ and $\vec{V}_{\mathcal{H},\mathrm{raw}}$. A comparison with the recoil velocity $\vec{V}_\mathcal{F}$ as computed for surrogate remnant models is also shown. The upper plot shows the absolute difference in magnitude. For reference, the value of V_∞ has been plotted as well. The lower plot shows the misalignment $\sin\Delta\Theta$, where $\Delta\Theta$ is the angle between the one of the recoil velocity vectors and $\vec{V}_\infty$. For most systems, errors in the methods used to compute the recoil velocity dominate over the numerical resolution.

the definition of the simulation coordinates. As such, it is not expected that a velocity measured with respect to some local coordinates will be comparable to that same velocity measured with respect to an entirely different coordinate system set up on $\mathscr{I}^+$. In fact, it has been shown that the naive choice of retarded time $u = t - r_*$ in simulation coordinates (where r_* is the radial tortoise

coordinate) actually fails to parametrize null rays for BBH spacetimes [46, 90].

The CoM drift during the simulation only complicates the issue. The black hole remnant of a system with no expected recoil velocity may still have an apparent horizon with some coordinate velocity because of this drift. In this case, we would obtain a misleading value of $\vec{V}_\mathcal{H}$ for systems with recoil velocities expected to be minimal or zero. Applying the boost from the CoM correction to $\vec{V}_\mathcal{H}$ is expected to mitigate this particular issue. To do this, we evaluate the horizon trajectory recoil velocity $\vec{V}_{\mathcal{H},\mathrm{raw}}$ with respect to the CoM drift velocity $\vec{V}_{\mathrm{CoM}}$ using relativistic velocity addition,

$$
\vec{V}_\mathcal{H} = \frac{1}{1 - \left(\vec{V}_{\mathrm{CoM}} \cdot \vec{V}_{\mathcal{H},\mathrm{raw}}\right)} \left(\frac{\vec{V}_{\mathcal{H},\mathrm{raw}}}{\gamma} - \vec{V}_{\mathrm{CoM}} \right.
$$
$$
\left. + \frac{\gamma}{1 + \gamma} \left(\vec{V}_{\mathrm{CoM}} \cdot \vec{V}_{\mathcal{H},\mathrm{raw}} \right) \vec{V}_{\mathrm{CoM}} \right). \tag{25}
$$

The CoM drift also affects the measurement of the recoil velocity from asymptotic data, if the asymptotic data is not given the appropriate boost and translation to correct for the CoM drift. However, applying a CoM correction to asymptotic data is straightforward and is routinely performed for all waveforms in the SXS waveform catalog [22]. We can therefore expect the most reliable recoil velocity to be determined by the CoM-corrected asymptotic data, $\vec{V}_\infty$. In the following analysis, we also include the recoil velocities computed without the CoM correction ($\vec{V}_{\infty,\mathrm{raw}}$ and $\vec{V}_{\mathcal{H},\mathrm{raw}}$) and the recoil velocity $\vec{V}_\mathcal{F}$ as computed for surrogate remnant models in Eq. (18).

In the upper plot of Fig. 3, we compare the magnitudes of the different measurements of the recoil velocity against the CoM-corrected asymptotic measurement V_∞. The lower plot of Fig. 3 shows the misalignment of the directions of the different recoil velocity measurements compared to $\vec{V}_\infty$. The angle between one of the recoil velocity measurements with $\vec{V}_\infty$ is given by $\Delta\Theta$.

The first four systems, (q1_aligned_chi0_2, q1_aligned_chi0_6, q1_aligned_chi0_4, q1_nospin), are expected to have zero recoil velocity because of the symmetry of the systems. Instead, we see that $V_{\mathcal{H},\mathrm{raw}}$ and $V_{\infty,\mathrm{raw}}$ for these systems are still as high as 10^{-8} (with $c = 1$). When using the CoM-corrected data, we find the much smaller recoil velocity of roughly 10^{-10}. When the recoil velocity is not substantially larger than the velocity of the CoM drift, we can expect a large relative error in both $V_{\mathcal{H},\mathrm{raw}}$ and $V_{\infty,\mathrm{raw}}$.

For the other nine systems, the recoil velocity should be much larger than the velocity of the CoM drift, so CoM correction is expected to have little effect. Indeed we find a relative difference of $\mathcal{O}(10^{-2})$ in the recoil velocity determined from horizon trajectory, regardless of CoM correction. For $V_{\infty,\mathrm{raw}}$, we see even smaller relative differences down to $\mathcal{O}(10^{-4})$ for systems with high recoil velocity. The large relative difference for $V_\mathcal{H}$ highlights

the overall lack of reliability in using horizon trajectory for determining recoil velocity, even when CoM-corrected.

For the systems with nonzero expected recoil velocity, we find that the magnitude of the recoil velocity $V_{\mathcal{F}}$ agrees with V_{∞} better than $V_{\mathcal{H}}$ does by up to two orders of magnitude in some cases. Only for the systems with no expected recoil does $V_{\mathcal{H}}$ outperform $V_{\mathcal{F}}$, which is most likely due to the lack of precision in choosing the integration constant for $V_{\mathcal{F}}$, cf. Eq. (18). When the numerical error is taken into account, we can see that there is a noticeable improvement that can be made by using V_{∞} instead of $V_{\mathcal{F}}$ for most systems. However, surrogate remnant models are currently using numerical resolutions even coarser than "LowRes", so such an improvement would be important only for future models.

The CoM correction also does not have a significant impact on the direction of the recoil velocity. We can see that $\hat{V}_{\infty,\text{raw}}$ is more aligned with $\hat{V}_{\infty}$ than $\hat{V}_{\mathcal{H}}$ is, even though the latter is CoM-corrected. On the other hand, when we consider the misalignment of the recoil velocity from the different measurements, the differences here are at or below the error from numerical resolution. Only for the q1_superkick system do we find that the CoM correction makes an improvement above numerical resolution.

C. Spin Comparison

To get the dimensionless spin of the black hole from the Bondi angular momentum, we compute the angular momentum in the center of momentum (CoMom) frame. If the asymptotic data is not in a CoMom frame, then the values that would be reported as spin would contain contributions from the orbital part of the angular momentum or be Lorentz transformed from the recoil velocity. Even systems with no expected recoil velocity would still be in a non-CoMom frame because of the CoM drift. However, for these special cases, the CoM correction itself would transform the asymptotic data to a CoMom frame. For all other systems, we will be far from a CoMom frame even with a CoM correction. In general, we need to apply the procedure described in Sec. II B to compute the dimensionless spin vector of the remnant $\vec{\chi}_{\infty}$.

A comparison of the remnant spin computed from the horizon, $\vec{\chi}_{\mathcal{H}}$, and from the asymptotic data, $\vec{\chi}_{\infty}$, is presented in Fig. 4. All the asymptotic data have been CoM-corrected. In the same figure, we also present a comparison of $\chi_{\mathcal{H}}$ and J_{∞}/M_{∞}^2 (i.e. the angular momentum computed only in the CoM frame, not necessarily in a CoMom frame) to demonstrate the importance of using a CoMom frame. Any differences in the comparison between $\vec{\chi}_{\mathcal{H}}$ and $\vec{\chi}_{\infty}$ and between $\vec{\chi}_{\mathcal{H}}$ and $\vec{J}_{\infty}/M_{\infty}^2$ would be due to $\vec{J}_{\infty}$ being computed in an undesirable frame. We need to divide J_{∞} by M_{∞}^2 in to render it dimensionless for comparing to the spin magnitude.

In general, there is remarkable agreement between the asymptotic and horizon-based spin vectors, $\vec{\chi}_{\infty}$ and
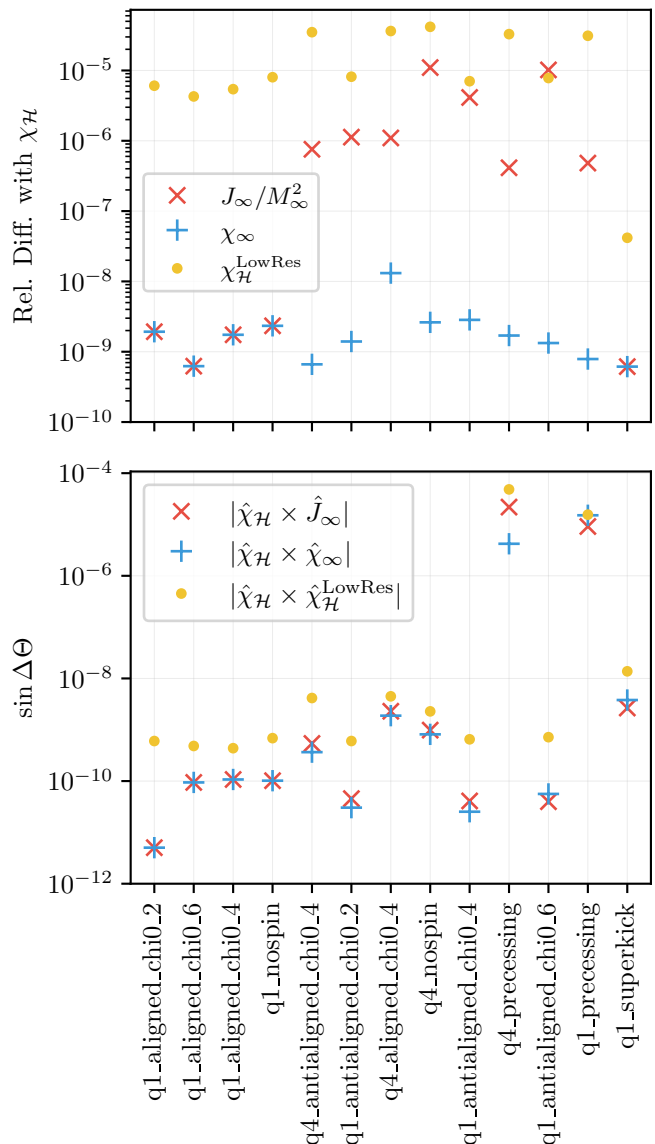

FIG. 4. A comparison of the dimensionless remnant spin computed from the apparent horizon and asymptotic data. The upper plot shows the relative difference of spin magnitudes $\chi_{\mathcal{H}}$ and χ_{∞}. It also shows the relative difference between $\chi_{\mathcal{H}}$ and the magnitude of the dimensionless angular momentum J_{∞}/M_{∞}^2. The lower plot shows the misalignment $\sin\Delta\Theta$ between the $\hat{\chi}_{\mathcal{H}}$ and $\hat{\chi}_{\infty}$ and between $\hat{\chi}_{\mathcal{H}}$ and $\hat{J}_{\infty}$, where $\Delta\Theta$ is the angle between the vectors. These plots show that the error in the spin vector is dominated by numerical resolution.

$\vec{\chi}_{\mathcal{H}}$. The relative difference in the magnitude is typically $\mathcal{O}(10^{-9})$, and the misalignment $\sin\Delta\Theta$ is below $\mathcal{O}(10^{-8})$ for nonprecessing systems, where $\Delta\Theta$ is now the angle between the spin vectors. The points representing $\hat{\chi}_{\infty}$ and $\hat{J}_{\infty}$ in the lower plot (but not the upper plot) are very similar to each other in all cases. Therefore, transforming to the CoMom frame does not seem to make a large impact on the direction of the spin vector.

There is a noticeably larger misalignment between the asymptotic and horizon-based spin vectors for precessing

systems. For these two systems, the final spin is still predominantly in the $+\hat{z}$ direction. Since both $\vec{\chi}_\infty$ and $\vec{\chi}_\mathcal{H}$ should produce precise spin measurements, one possible source of discrepancy could be that they do not correspond to the same definition of the spin axis [30]. It is also likely, however, that the difference is caused by the lack of numerical resolution for these two runs compared to the other systems, since the difference is on the same order as the difference between the high and low resolution $\vec{\chi}_\mathcal{H}$.

The four systems with no recoil velocity after a CoM correction, (q1_aligned_chi0_2, q1_aligned_chi0_6, q1_aligned_chi0_4, q1_nospin), show no improvement from the CoMom correction. This is because the remnants are already in a CoMom frame. The other systems with remnants that are not in a CoMom frame show an improvement of two to four orders of magnitude by using Eq. (15) to compute the spin vector. The only exception to this is the q1_superkick system. The symmetries of this system result in a trajectory, velocity, and spin vector pointing almost exactly along the $+z$ axis. Therefore, even when we are not in the CoMom frame the orbital angular momentum and the component of the velocity orthogonal to the spin are both negligible for this system.

The dominant source of error in determining the remnant spin is still the numerical resolution. Even the largest differences in spin measurements are not above the numerical error. Consequently, the arguments presented in Sec. II C appear to hold very well for the remnant spin.

IV. CONCLUSION

The availability of accurate and reliable measurements of quantities at $\mathscr{I}^+$ from numerical simulations has opened up a new arena of applications and analysis tools provided by the BMS group. In this paper, we have explored using asymptotic data to provide accurate measurements of the mass, spin, and recoil velocity of a remnant black hole from a set of numerically evolved binary black hole mergers. These asymptotic remnant properties have been compared against independent quasi-local measurements from the remnant apparent horizon.

Overall, there is remarkable agreement between the mass and spin measured from the remnant apparent horizon and on the boundary of the spacetime. For nearly equal-mass BBH systems with low total spin, the relative difference between the two measurements of remnant mass is around $\mathcal{O}(10^{-7})$, and for more extreme systems the relative difference does not rise above $\mathcal{O}(10^{-5})$.

The agreement on the spin is even better. By computing the spin from the angular momentum evaluated in a CoMom frame, the horizon-based and asymptotic spin magnitudes agree to $\mathcal{O}(10^{-9})$, with only one of our 13 chosen example BBH configurations showing a relative difference as high as $\mathcal{O}(10^{-8})$. The misalignment $\sin \Delta \Theta$ between the horizon-based and asymptotic spin vectors is $\mathcal{O}(10^{-6})$ for precessing systems and consistently between $\mathcal{O}(10^{-11})$ and $\mathcal{O}(10^{-8})$ for nonprecessing systems.

Although evaluating the angular momentum in a CoMom frame does not have a large impact on the direction of the spin vector, using a CoMom frame affords a considerable improvement on the spin magnitude for systems without a high degree of symmetry. For such systems, evaluating the angular momentum in the CoMom frame lowered the relative difference between the horizon-based and asymptotic spin magnitude by up to four orders of magnitude.

The recoil velocity showed worse agreement between the horizon-based and asymptotic measurements. The BBH system's CoM is known to drift during the course of the simulation, which erroneously contributes to naive measurements of the recoil velocity. However, this effect is not a dominant source of error when the recoil velocity is much larger than the CoM drift velocity. For these cases, the relative difference between the horizon-based and asymptotic recoil velocity magnitude is around $\mathcal{O}(10^{-2})$. For systems with no expected recoil velocity, the computed recoil velocities are two orders of magnitude smaller when a CoM correction has been applied.

The SXS waveform catalog does not currently apply a CoM correction to the coordinate recoil velocity. This correction is straightforward and computationally inexpensive to perform, and it will provide a significant improvement to the reported remnant velocity for highly symmetric BBH systems. However, as the complete set of asymptotic data becomes more widely available in the catalog, the CoM-corrected asymptotic recoil velocity $\vec{V}_\infty$ should be reported instead. To this end, an improved CoM correction is a high priority and would immediately yield a more precise measure of the recoil velocity.

Such an improved correction would have an important application for constructing surrogate remnant models, which compute a recoil velocity from the asymptotic strain alone. Although we have demonstrated that the procedure currently used in surrogate remnant models provides a recoil velocity that is generally closer to $\vec{V}_\infty$ than $\vec{V}_\mathcal{H}$ is, the precision is limited by a frame choice determined by time-averaging an oscillating quantity over a short interval. Using the asymptotic recoil velocity computed from asymptotic data would be far more reliable and robust for the construction of surrogates. A detailed comparison of how the two measurements of recoil velocity impact the results of surrogate remnant models is an avenue of future work.

Although the asymptotic recoil velocity should be more accurate than the horizon-based measurement, we can expect a far better agreement between the horizon-based and asymptotic measurements of remnant mass and spin, as we discussed in Sec. II C. As such, it cannot be determined from our analysis whether an asymptotic or a horizon-based measurement of mass and spin is more accurate. Rather, the comparison made here provides us with a consistency test for these two remnant properties, and this test is another valuable analysis tool for providing estimates of the error with regards to the underlying physics.

ACKNOWLEDGMENTS

Appendix: A Note on the Angular Momentum and Boost Charges

When defining the charges $\vec{J}_{\mathrm{B}}$ and $\vec{K}_{\mathrm{B}}$ in Eqs. (13) for computing the spin vector in Eq. (15), it is important to note that these charges are are not uniquely defined. The charges defined above are *adapted* to the Bondi frame in question [91], as described below. Consequently, if we supertranslate the frame, the charge transforms accordingly. However as we will see below, these ambiguities vanish for charges of interest in stationary spacetimes and hence they do not affect the remnant quantities.

First we discuss rotations. The angular momentum is adapted to the Bondi frame in the sense that the generators of the corresponding rotations $\vec{L}^a$ are taken to be tangential to the $u = \mathrm{const}$ surfaces at $\mathscr{I}^+$, hence the rotation does not transform the time coordinate.[8] However, consider a supertranslated foliation of constant $u' = u - \alpha(\theta, \phi)$. Then the rotations $\vec{L}'^a$ adapted to the new Bondi frame are given by

$$\vec{L}'^a = \vec{L}^a + (\vec{L}^b \nabla_b \alpha) n^a, \qquad (A.1)$$

with $n^a = (\partial_u)^a$.

Now, using the fact that the charge at $\mathscr{I}^+$ corresponding to a generator ξ is linear in ξ, we have that

$$\vec{J}'_{\mathrm{B}} = \vec{J}_{\mathrm{B}} + Q[(\vec{L}^b \nabla_b \alpha) n^a], \qquad (A.2)$$

where we used $Q[\vec{L}^a] = \vec{J}_{\mathrm{B}}$ and the charges are evaluated implicitly at some time u. Further we use

$$Q[f n^a] = \frac{1}{4\pi} \int f m \, d\Omega \qquad (A.3)$$

to evaluate the transformation of the adapted angular momentum [50]. Note that this leads to the familiar transformation of angular momentum under translations if α contains only $\ell = 1$ modes. The transformation is now generalized to supertranslations. While Eq. (A.2) leads to an ambiguity in the notion of angular momentum, as the spacetime approaches stationarity there is a simplification. If we are in the rest frame of the stationary spacetime we have that

$$m(\theta, \phi) = M_{\mathrm{B}}, \qquad (A.4)$$

that is $m(\theta, \phi)$ is a constant function. Because $(\vec{L}^b \nabla_b \alpha)$ has only $\ell \geq 1$ spherical harmonic components, at late times we find

$$Q[(\vec{L}^b \nabla_b \alpha) n^a] = \frac{1}{4\pi} \int (\vec{L}^b \nabla_b \alpha) M_{\mathrm{B}} \, d\Omega = 0. \qquad (A.5)$$

Hence, at late times we have

$$\vec{J}'_\infty = \vec{J}_\infty. \qquad (A.6)$$

Therefore the ambiguity in the definition of angular momentum is irrelevant for the analysis of remnants. Crucially, this is true only in the CoMom frame, where Eq. (A.4) holds. This explains why the argument in Sec. II C holds even though we did not use the azimuthal Killing vector to define the angular momentum: The angular momentum of the Killing vector is equal to that of any rotation around the same axis at $\mathscr{I}^+$.

Unlike rotations, boosts cannot be tangential to the $u = \mathrm{const}$ foliation. They can only be tangential at one time slice. Conventionally the generators adapted to a Bondi frame are defined to be the ones tangential to the $u = 0$ time slice. Thus the boost generators $\vec{\xi}^a$ transform under time translation, as is to be expected from special relativity. Also unlike rotations, the boost charge transforms in stationary spacetimes in the CoMom frame. This transformation does not concern us because the charge in Eq. (15), which is a linear combination of boost and rotation charges in the simulation frame, is precisely the charge corresponding to a rotation in the CoMom frame. Thus Eq. (15) does not transform under supertranslations.

---

[8] $\vec{L}^a$ is a list of three 4-vectors generating rotations in the x, y and z directions.

[1] R. Abbott *et al.* (LIGO Scientific, Virgo), GWTC-2: Compact Binary Coalescences Observed by LIGO and Virgo During the First Half of the Third Observing Run, arXiv:2010.14527 [gr-qc].

[2] B. P. Abbott *et al.* (LIGO Scientific, Virgo), GWTC-1: A

Gravitational-Wave Transient Catalog of Compact Binary Mergers Observed by LIGO and Virgo during the First and Second Observing Runs, Phys. Rev. X **9**, 031040 (2019), arXiv:1811.12907 [astro-ph.HE].

[3] B. P. Abbott *et al.* (LIGO Scientific, Virgo), Binary Black Hole Mergers in the first Advanced LIGO Observing Run, Phys. Rev. X **6**, 041015 (2016), [Erratum: Phys. Rev. X **8**, 039903 (2018)], arXiv:1606.04856 [gr-qc].

[4] B. P. Abbott *et al.* (LIGO Scientific, Virgo), Observation of Gravitational Waves from a Binary Black Hole Merger, Phys. Rev. Lett. **116**, 061102 (2016), arXiv:1602.03837 [gr-qc].

[5] D. Gerosa and A. Sesana, Missing black holes in brightest cluster galaxies as evidence for the occurrence of superkicks in nature, Mon. Not. R. Astron. Soc. **446**, 38 (2015), arXiv:1405.2072 [astro-ph.GA].

[6] M. Arca Sedda and M. Benacquista, Using final black hole spins and masses to infer the formation history of the observed population of gravitational wave sources, Mon. Not. R. Astron. Soc. **482**, 2991 (2019), arXiv:1806.01285 [astro-ph.GA].

[7] M. Volonteri, K. Gultekin, and M. Dotti, Gravitational recoil: effects on massive black hole occupation fraction over cosmic time, Mon. Not. R. Astron. Soc. **404**, 2143 (2010), arXiv:1001.1743 [astro-ph.CO].

[8] S. Komossa and D. Merritt, Gravitational Wave Recoil Oscillations of Black Holes: Implications for Unified Models of Active Galactic Nuclei, Astrophys. J. Lett. **689**, L89 (2008), arXiv:0811.1037 [astro-ph].

[9] M. Volonteri, M. Sikora, J.-P. Lasota, and A. Merloni, The evolution of active galactic nuclei and their spins, Astrophys. J. **775**, 94 (2013), arXiv:1210.1025 [astro-ph.HE].

[10] P. Amaro-Seoane, S. Konstantinidis, M. D. Freitag, M. C. Miller, and F. A. Rasio, Sowing the Seeds of Massive Black Holes in Small Galaxies: Young Clusters as the Building Blocks of Ultracompact Dwarf Galaxies, Astrophys. J. **782**, 97 (2014), arXiv:1211.6738 [astro-ph.CO].

[11] M. Volonteri, F. Haardt, and K. Gultekin, Compact massive objects in Virgo galaxies: the black hole population, Mon. Not. R. Astron. Soc. **384**, 1387 (2008), arXiv:0710.5770 [astro-ph].

[12] B. P. Abbott *et al.* (LIGO Scientific, Virgo), Tests of General Relativity with the Binary Black Hole Signals from the LIGO-Virgo Catalog GWTC-1, Phys. Rev. D **100**, 104036 (2019), arXiv:1903.04467 [gr-qc].

[13] B. P. Abbott *et al.* (LIGO Scientific, Virgo), Tests of general relativity with GW150914, Phys. Rev. Lett. **116**, 221101 (2016), [Erratum: Phys. Rev. Lett. **121**, 129902 (2018)], arXiv:1602.03841 [gr-qc].

[14] Z. Carson and K. Yagi, Parametrized and inspiral-merger-ringdown consistency tests of gravity with multiband gravitational wave observations, Phys. Rev. D **101**, 044047 (2020), arXiv:1911.05258 [gr-qc].

[15] A. Ghosh, N. K. Johnson-Mcdaniel, A. Ghosh, C. K. Mishra, P. Ajith, W. Del Pozzo, C. P. L. Berry, A. B. Nielsen, and L. London, Testing general relativity using gravitational wave signals from the inspiral, merger and ringdown of binary black holes, Classical Quant. Grav. **35**, 014002 (2018), arXiv:1704.06784 [gr-qc].

[16] R. Brito, A. Buonanno, and V. Raymond, Black-hole Spectroscopy by Making Full Use of Gravitational-Wave Modeling, Phys. Rev. D **98**, 084038 (2018), arXiv:1805.00293 [gr-qc].

[17] G. Carullo *et al.*, Empirical tests of the black hole no-hair conjecture using gravitational-wave observations, Phys. Rev. D **98**, 104020 (2018), arXiv:1805.04760 [gr-qc].

[18] M. Isi, M. Giesler, W. M. Farr, M. A. Scheel, and S. A. Teukolsky, Testing the no-hair theorem with GW150914, Phys. Rev. Lett. **123**, 111102 (2019), arXiv:1905.00869 [gr-qc].

[19] M. Pürrer and C.-J. Haster, Gravitational waveform accuracy requirements for future ground-based detectors, Phys. Rev. Research **2**, 023151 (2020).

[20] K. Jani, J. Healy, J. A. Clark, L. London, P. Laguna, and D. Shoemaker, Georgia Tech Catalog of Gravitational Waveforms, Classical Quant. Grav. **33**, 204001 (2016), arXiv:1605.03204 [gr-qc].

[21] E. A. Huerta *et al.*, Physics of eccentric binary black hole mergers: A numerical relativity perspective, Phys. Rev. D **100**, 064003 (2019), arXiv:1901.07038 [gr-qc].

[22] M. Boyle *et al.*, The SXS Collaboration catalog of binary black hole simulations, Classical Quant. Grav. **36**, 195006 (2019), arXiv:1904.04831 [gr-qc].

[23] J. Healy and C. O. Lousto, Third RIT binary black hole simulations catalog, Phys. Rev. D **102**, 104018 (2020), arXiv:2007.07910 [gr-qc].

[24] L. B. Szabados, Quasi-local energy-momentum and angular momentum in general relativity, Living Rev. Relativity **12**, 4 (2009).

[25] S. Bhagwat, M. Okounkova, S. W. Ballmer, D. A. Brown, M. Giesler, M. A. Scheel, and S. A. Teukolsky, On choosing the start time of binary black hole ringdowns, Phys. Rev. D **97**, 104065 (2018), arXiv:1711.00926 [gr-qc].

[26] R. Owen, Degeneracy measures for the algebraic classification of numerical spacetimes, Phys. Rev. D **81**, 124042 (2010), arXiv:1004.3768 [gr-qc].

[27] R. Owen, The Final Remnant of Binary Black Hole Mergers: Multipolar Analysis, Phys. Rev. D **80**, 084012 (2009), arXiv:0907.0280 [gr-qc].

[28] M. A. Scheel, M. Giesler, D. A. Hemberger, G. Lovelace, K. Kuper, M. Boyle, B. Szilágyi, and L. E. Kidder, Improved methods for simulating nearly extremal binary black holes, Classical Quant. Grav. **32**, 105009 (2015), arXiv:1412.1803 [gr-qc].

[29] C. O. Lousto and Y. Zlochower, Black hole binary remnant mass and spin: A new phenomenological formula, Phys. Rev. D **89**, 104052 (2014), arXiv:1312.5775 [gr-qc].

[30] R. Owen, A. S. Fox, J. A. Freiberg, and T. P. Jacques, Black Hole Spin Axis in Numerical Relativity, Phys. Rev. D **99**, 084031 (2019), arXiv:1708.07325 [gr-qc].

[31] J. L. Jaramillo and E. Gourgoulhon, Mass and Angular Momentum in General Relativity, Fundam. Theor. Phys. **162**, 87 (2011), arXiv:1001.5429 [gr-qc].

[32] B. Krishnan, Fundamental properties and applications of quasi-local black hole horizons, Classical Quant. Grav. **25**, 114005 (2008), arXiv:0712.1575 [gr-qc].

[33] B. Krishnan, C. O. Lousto, and Y. Zlochower, Quasilocal linear momentum in black-hole binaries, Phys. Rev. D **76**, 081501(R) (2007), arXiv:0707.0876 [gr-qc].

[34] O. Dreyer, B. Krishnan, D. Shoemaker, and E. Schnetter, Introduction to isolated horizons in numerical relativity, Phys. Rev. D **67**, 024018 (2003), arXiv:gr-qc/0206008.

[35] J. L. Jaramillo, R. P. Macedo, P. Moesta, and L. Rezzolla, Black-hole horizons as probes of black-hole dynamics. I. Post-merger recoil in head-on collisions, Phys. Rev. D **85**, 084030 (2012), arXiv:1108.0060 [gr-qc].

[36] G. Compère and A. Fiorucci, Advanced Lectures on General Relativity, arXiv:1801.07064 [hep-th].

[37] J. Stewart, *Advanced General Relativity*, Cambridge Monographs on Mathematical Physics (Cambridge University Press, Cambridge, England, 1993).

[38] V. Varma, D. Gerosa, L. C. Stein, F. Hébert, and H. Zhang, High-accuracy mass, spin, and recoil predictions of generic black-hole merger remnants, Phys. Rev. Lett. **122**, 011101 (2019), arXiv:1809.09125 [gr-qc].

[39] D. Gerosa, F. Hébert, and L. C. Stein, Black-hole kicks from numerical-relativity surrogate models, Phys. Rev. D **97**, 104049 (2018), arXiv:1802.04276 [gr-qc].

[40] J. Healy, C. O. Lousto, and Y. Zlochower, Remnant mass, spin, and recoil from spin aligned black-hole binaries, Phys. Rev. D **90**, 104004 (2014), arXiv:1406.7295 [gr-qc].

[41] C. O. Lousto, M. Campanelli, Y. Zlochower, and H. Nakano, Remnant Masses, Spins and Recoils from the Merger of Generic Black-Hole Binaries, Classical Quant. Grav. **27**, 114006 (2010), arXiv:0904.3541 [gr-qc].

[42] C. O. Lousto and Y. Zlochower, A Practical formula for the radiated angular momentum, Phys. Rev. D **76**, 041502(R) (2007), arXiv:gr-qc/0703061.

[43] V. Varma, M. Isi, and S. Biscoveanu, Extracting the Gravitational Recoil from Black Hole Merger Signals, Phys. Rev. Lett. **124**, 101104 (2020), arXiv:2002.00296 [gr-qc].

[44] N. Deppe, W. Throwe, L. E. Kidder, N. L. Fischer, C. Armaza, G. S. Bonilla, F. Hébert, P. Kumar, G. Lovelace, J. Moxon, E. O'Shea, H. P. Pfeiffer, M. A. Scheel, S. A. Teukolsky, I. Anantpurkar, M. Boyle, F. Foucart, M. Giesler, D. A. B. Iozzo, I. Legred, D. Li, A. Macedo, D. Melchor, M. Morales, T. Ramirez, H. R. Rüter, J. Sanchez, S. Thomas, and T. Wlodarczyk, SpECTRE, doi: 10.5281/zenodo.4290405 (2020).

[45] J. Moxon, M. A. Scheel, and S. A. Teukolsky, Improved Cauchy-characteristic evolution system for high-precision numerical relativity waveforms, Phys. Rev. D **102**, 044052 (2020), arXiv:2007.01339 [gr-qc].

[46] D. A. B. Iozzo, M. Boyle, N. Deppe, J. Moxon, M. A. Scheel, L. E. Kidder, H. P. Pfeiffer, and S. A. Teukolsky, Extending gravitational wave extraction using Weyl characteristic fields, Phys. Rev. D **103**, 024039 (2021), arXiv:2010.15200 [gr-qc].

[47] H. Bondi, M. G. J. Van der Burg, and A. W. K. Metzner, Gravitational waves in general relativity, VII. Waves from axi-symmetric isolated system, Proc. R. Soc. A **269**, 21 (1962).

[48] R. K. Sachs, Gravitational waves in general relativity viii. waves in asymptotically flat space-time, Proc. R. Soc. A **270**, 103 (1962).

[49] L. A. Gómez López and G. D. Quiroga, Asymptotic structure of spacetime and the Newman-Penrose formalism: a brief review, Rev. Mex. Fis. **63**, 275 (2017), arXiv:1711.11381 [gr-qc].

[50] T. Dray, Momentum flux at null infinity, Classical Quant. Grav. **2**, L7 (1985).

[51] T. Dray and M. Streubel, Angular momentum at null infinity, Classical Quant. Grav. **1**, 15 (1984).

[52] M. Streubel, "Conserved" quantities for isolated gravitational systems, Gen. Relativ. Gravit. **9**, 551 (1978).

[53] SXS Gravitational Waveform Database, https://data.black-holes.org/waveforms.

[54] Spectral Einstein Code, https://www.black-holes.org/code/SpEC.html.

[55] M. C. Babiuc, B. Szilágyi, J. Winicour, and Y. Zlochower, Characteristic extraction tool for gravitational waveforms, Phys. Rev. D **84**, 044057 (2011), arXiv:1011.4223 [gr-qc].

[56] C. Reisswig, N. T. Bishop, D. Pollney, and B. Szilágyi, Characteristic extraction in numerical relativity: binary black hole merger waveforms at null infinity, Classical Quant. Grav. **27**, 075014 (2010), arXiv:0912.1285 [gr-qc].

[57] C. Reisswig, N. T. Bishop, D. Pollney, and B. Szilágyi, Unambiguous determination of gravitational waveforms from binary black hole mergers, Phys. Rev. Lett. **103**, 221101 (2009), arXiv:0907.2637 [gr-qc].

[58] C. J. Woodford, M. Boyle, and H. P. Pfeiffer, Compact Binary Waveform Center-of-Mass Corrections, Phys. Rev. D **100**, 124010 (2019), arXiv:1904.04842 [gr-qc].

[59] A. Nagar, G. Riemenschneider, and G. Pratten, Impact of Numerical Relativity information on effective-one-body waveform models, Phys. Rev. D **96**, 084045 (2017), arXiv:1703.06814 [gr-qc].

[60] S. Ossokine, F. Foucart, H. P. Pfeiffer, M. Boyle, and B. Szilágyi, Improvements to the construction of binary black hole initial data, Classical Quant. Grav. **32**, 245010 (2015), arXiv:1506.01689 [gr-qc].

[61] S. Ossokine, L. E. Kidder, and H. P. Pfeiffer, Precession-tracking coordinates for simulations of compact-object-binaries, Phys. Rev. D **88**, 084031 (2013), arXiv:1304.3067 [gr-qc].

[62] M. Boyle, Transformations of asymptotic gravitational-wave data, Phys. Rev. D **93**, 084031 (2016), arXiv:1509.00862 [gr-qc].

[63] O. M. Moreschi, On angular momentum at future null infinity, Classical Quant. Grav. **3**, 503 (1986).

[64] G. Lovelace, R. Owen, H. P. Pfeiffer, and T. Chu, Binary-black-hole initial data with nearly-extremal spins, Phys. Rev. D **78**, 084017 (2008), arXiv:0805.4192 [gr-qc].

[65] G. B. Cook and B. F. Whiting, Approximate Killing Vectors on S^2, Phys. Rev. D **76**, 041501(R) (2007), arXiv:0706.0199 [gr-qc].

[66] R. Penrose and W. Rindler, *Spinors and Space-Time: Volume 1, Two-Spinor Calculus and Relativistic Fields*, Cambridge Monographs on Mathematical Physics (Cambridge University Press, Cambridge, England, 1984).

[67] D. Christodoulou and R. Ruffini, Reversible transformations of a charged black hole, Phys. Rev. D **4**, 3552 (1971).

[68] R. Geroch, A. Held, and R. Penrose, A space-time calculus based on pairs of null directions, J. Math. Phys. (N.Y.) **14**, 874 (1973).

[69] F. M., *Special Relativity and How it Works* (Wiley-VCH, Weinheim, 2008).

[70] M. Boyle, D. Hemberger, D. A. B. Iozzo, G. Lovelace, S. Ossokine, H. P. Pfeiffer, M. A. Scheel, L. C. Stein, C. J. Woodford, A. B. Zimmerman, N. Afshari, K. Barkett, J. Blackman, K. Chatziioannou, T. Chu, N. Demos, N. Deppe, S. E. Field, N. L. Fischer, E. Foley, H. Fong, A. Garcia, M. Giesler, F. Hebert, I. Hinder, R. Katebi, H. Khan, L. E. Kidder, P. Kumar, K. Kuper, H. Lim, M. Okounkova, T. Ramirez, S. Rodriguez, H. R. Rüter, P. Schmidt, B. Szilágyi, S. A. Teukolsky, V. Varma, and M. Walker, The SXS collaboration catalog of binary black hole simulations, Classical Quant. Grav. **36**, 195006 (2019), arXiv:1904.04831 [gr-qc].

[71] O. Sarbach and M. Tiglio, Gauge-invariant perturbations of Schwarzschild black holes in horizon-penetrating coordinates, Phys. Rev. D **64**, 084016 (2001), arXiv:gr-qc/0104061.

[72] T. Regge and J. A. Wheeler, Stability of a Schwarzschild Singularity, Phys. Rev. **108**, 1063 (1957).

[73] F. J. Zerilli, Effective Potential for Even-Parity Regge-Wheeler Gravitational Perturbation Equations, Phys. Rev. Lett. **24**, 737 (1970).

[74] M. Ruiz, R. Takahashi, M. Alcubierre, and D. Nunez, Multipole expansions for energy and momenta carried by gravitational waves, Gen. Relativ. Gravit. **40**, 2467 (2008), arXiv:0707.4654 [gr-qc].

[75] A. Ashtekar and B. Krishnan, Dynamical horizons and their properties, Phys. Rev. D **68**, 104030 (2003), arXiv:gr-qc/0308033.

[76] J. L. Jaramillo, R. P. Macedo, P. Moesta, and L. Rezzolla, Towards a cross-correlation approach to strong-field dynamics in black hole spacetimes, AIP Conf. Proc. **1458**, 158 (2012), arXiv:1205.3902 [gr-qc].

[77] J. Lee and R. M. Wald, Local symmetries and constraints, J. Math. Phys. (N.Y.) **31**, 725 (1990).

[78] R. M. Wald, Black hole entropy is the Noether charge, Phys. Rev. D **48**, R3427 (1993), arXiv:gr-qc/9307038.

[79] V. Iyer and R. M. Wald, A comparison of Noether charge and Euclidean methods for computing the entropy of stationary black holes, Phys. Rev. D **52**, 4430 (1995), arXiv:gr-qc/9503052.

[80] R. M. Wald and A. Zoupas, A general definition of 'conserved quantities' in general relativity and other theories of gravity, Phys. Rev. D **61**, 084027 (2000), arXiv:gr-qc/9911095.

[81] V. Iyer and R. M. Wald, Some properties of Noether charge and a proposal for dynamical black hole entropy, Phys. Rev. D **50**, 846 (1994), arXiv:gr-qc/9403028.

[82] R. P. Geroch and J. Winicour, Linkages in general relativity, J. Math. Phys. (N.Y.) **22**, 803 (1981).

[83] K. Mitman *et al.*, Adding gravitational memory to waveform catalogs using BMS balance laws, Phys. Rev. D **103**, 024031 (2021), arXiv:2011.01309 [gr-qc].

[84] L. Lindblom and B. Szilagyi, An Improved Gauge Driver for the GH Einstein System, Phys. Rev. D **80**, 084019 (2009), arXiv:0904.4873 [gr-qc].

[85] B. Szilagyi, L. Lindblom, and M. A. Scheel, Simulations of Binary Black Hole Mergers Using Spectral Methods, Phys. Rev. D **80**, 124010 (2009), arXiv:0909.3557 [gr-qc].

[86] M. W. Choptuik and F. Pretorius, Ultra Relativistic Particle Collisions, Phys. Rev. Lett. **104**, 111101 (2010), arXiv:0908.1780 [gr-qc].

[87] M. Boyle, D. A. B. Iozzo, and L. C. Stein, moble/scri: v1.2, `https://github.com/moble/scri` (2020).

[88] M. Boyle, Angular velocity of gravitational radiation from precessing binaries and the corotating frame, Phys. Rev. D **87**, 104006 (2013), arXiv:1302.2919 [gr-qc].

[89] M. Boyle, L. E. Kidder, S. Ossokine, and H. P. Pfeiffer, Gravitational-wave modes from precessing black-hole binaries, arXiv:1409.4431 [gr-qc].

[90] M. Boyle and A. H. Mroue, Extrapolating gravitational-wave data from numerical simulations, Phys. Rev. D **80**, 124045 (2009), arXiv:0905.3177 [gr-qc].

[91] A. Ashtekar, T. De Lorenzo, and N. Khera, Compact binary coalescences: The subtle issue of angular momentum, Phys. Rev. D **101**, 044005 (2020), arXiv:1910.02907 [gr-qc].